Volume 13
Number 40
28 October 2022
Pages 11699–11952

Chemical Science

rsc.li/chemical-science

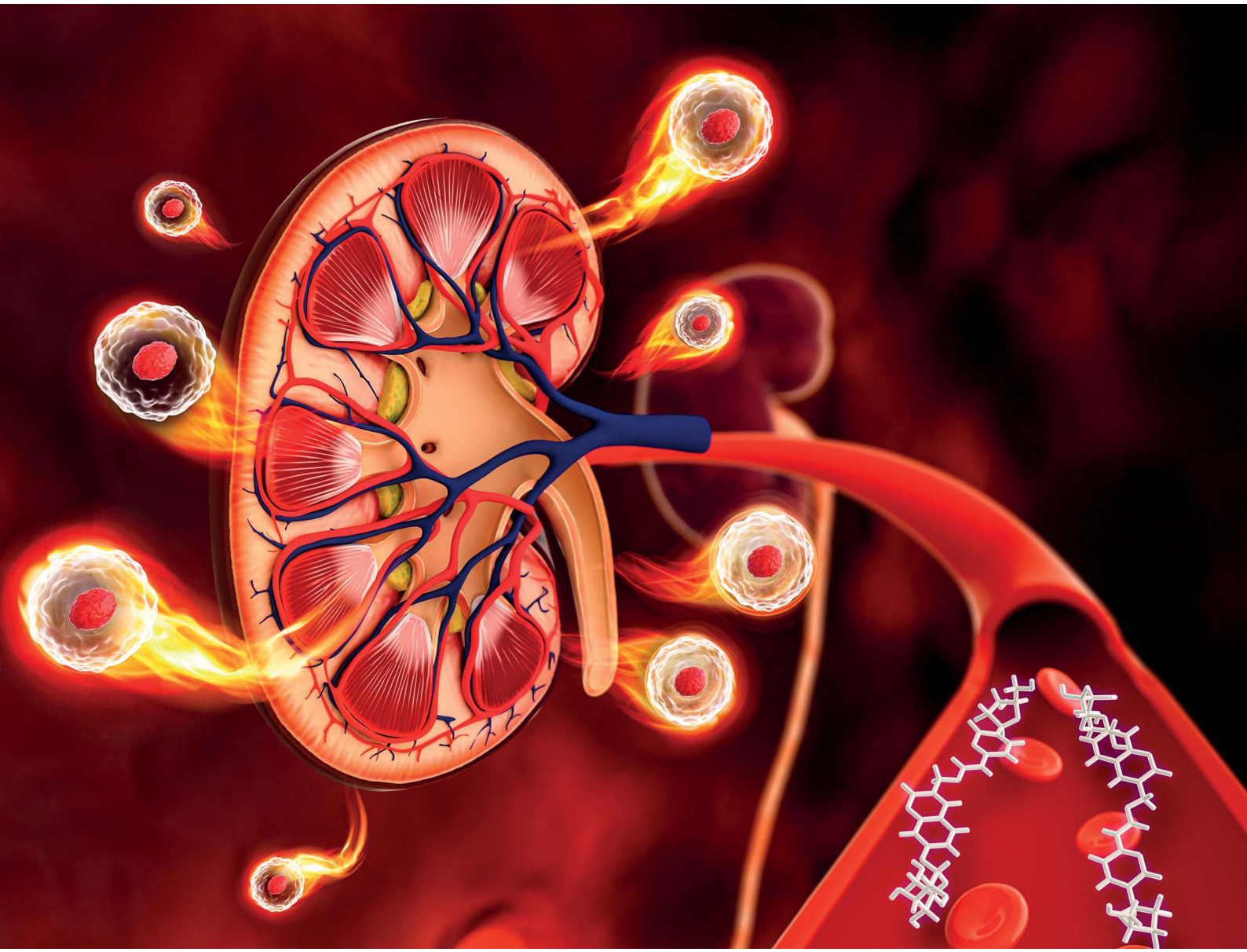

ISSN 2041-6539

ROYAL SOCIETY OF CHEMISTRY

EDGE ARTICLE

Yuan Guo, Jian Li *et al.*

A senolysis-based theragnostic prodrug strategy towards chronic renal failure

Chemical Science

ROYAL SOCIETY OF CHEMISTRY

EDGE ARTICLE

View Article Online
View Journal | View Issue

Cite this: *Chem. Sci.*, 2022, **13**, 11738

All publication charges for this article have been paid for by the Royal Society of Chemistry

Received 23rd June 2022
Accepted 15th September 2022

DOI: 10.1039/d2sc03525a

rsc.li/chemical-science

A senolysis-based theragnostic prodrug strategy towards chronic renal failure†

Yihe Song, ‡[a] Xinming Li, ‡[a] Donglei Shi, ‡[ab] Tianyue Sun, [a] Wenwen Liu, [c] Xiaokang Li, [a] Sicong Qiao, [a] Xin Chen, [a] Yuan Guo *[b] and Jian Li *[acde]

Selective elimination of senescent cells (senolysis) has become a promising therapeutic strategy for the management of chronic renal failure (CRF), but the senolytic molecular pathways towards CRF therapy are limited. Here, we present for the first time a senescence-associated β-galactosidase (SA-β-gal) activatable theragnostic prodrug strategy to pertinently and effectively treat CRF in mice with the aid of fluorescence-guided senolysis. The signs of premature senescence, including the overexpression of β-gal, have been found in kidneys of mice with CRF, making this enzyme particularly suitable as a trigger of prodrugs for CRF therapy. With this unique design, our pioneering prodrug **TSPD** achieved the activation of a fluorophore for tracking and the specific release of the parent drug, gemcitabine, in β-gal-enriched cells after activation with SA-β-gal. In mice with CRF, abdominal administration of **TSPD** was effective for improvement of the kidney functions, supporting the feasibility of the SA-β-gal-dependent senolysis therapy towards CRF.

Introduction

Chronic renal failure (CRF), also termed chronic kidney disease, is marked by a progressive decline in the renal structure and function, which ultimately leads to the need for kidney transplantation therapy.[1,2] CRF has become a global pandemic that affects at least 10% of the population worldwide and results in millions of deaths every year.[3,4] In recent decades, the morbidity and mortality rate of CRF have been increasing in aged population, especially in those suffering from age-related diseases, such as diabetes and hypertension.[5] Acute kidney injury (AKI), a sudden loss of kidney excretory function, has been proposed to be a great risk of kidney damage and progression of CRF, and the abnormal repair after AKI will further affect kidney functions in humans.[6–9] Furthermore, oxidative stress and premature cellular senescence occur in kidneys after injury, particularly in those of patients with CRF.[10–12] Under physiological conditions, transient development of senescence is considered to be a safeguard to prevent the accumulation of damaged cells and the occurrence of cancer,[13,14] whereas the abnormal accumulation of senescent cells (SNCs) caused by premature senescence is detrimental to renal functions and can even lead to organ failure.[15,16] This is considered to be caused by the damage of surrounding normal cells by proinflammatory cytokines and chemokines secreted by non-functional SNCs, termed senescence-associated secretory phenotypes (SASPs).[17,18] As such, the selective death induction of SNCs (senolysis) increasingly becomes a pharmacological approach to alleviate these pathologies associated with the accumulation of SNCs.[19] Experiments in mice support that the administration of senolytic drugs (senolytics), such as ABT-263 or the dasatinib/quercetin cocktail, can ameliorate chronic renal disease and promote kidney repair after AKI.[20,21] Obviously, SNCs have become an emerging therapeutic target for the treatment of CRF, and the challenge then becomes how to create effective molecular pathways for senolysis-based CRF therapy.

Since signs of senescence have been found in kidneys of mice with CRF, hallmarks of cellular senescence are also suitable for identifying CRF. So far, a series of senescence biomarkers have been proposed, such as $p16^{INK4A}$, lamin B1, p53, p21, γH2AX, senescence-associated β-galactosidase (SA-β-gal) and so on.[22–25] Among them, SA-β-gal, the most reliable protein marker, has been widely used *in vitro* and *in vivo* for the

[a]*State Key Laboratory of Bioreactor Engineering, Shanghai Frontiers Science Center of Optogenetic Techniques for Cell Metabolism, Frontiers Science Center for Materiobiology and Dynamic Chemistry, Shanghai Key Laboratory of New Drug Design, School of Pharmacy, East China University of Science and Technology, Shanghai 200237, China. E-mail: jianli@ecust.edu.cn*

[b]*Key Laboratory of Synthetic and Natural Functional Molecule of the Ministry of Education, College of Chemistry and Materials Science, Northwest University, Xi'an 710127, China. E-mail: guoyuan@nwu.edu.cn*

[c]*Key Laboratory of Tropical Biological Resources of Ministry of Education, College of Pharmacy, Hainan University, Haikou 570228, Hainan, China*

[d]*Clinical Medicine Scientific and Technical Innovation Center, Shanghai Tenth People's Hospital, Tongji University School of Medicine, Shanghai 200092, China*

[e]*Yunnan Key Laboratory of Screening and Research on Anti-pathogenic Plant Resources from West Yunnan, College of Pharmacy, Dali University, Dali 671000, China*

† Electronic supplementary information (ESI) available: Experimental section, additional figures, synthetic procedures, and original spectra of new compounds. See https://doi.org/10.1039/d2sc03525a

‡ These authors contributed equally to this work.

recognition of different types of SNC.[26] Of note, this enzyme located in lysosomes has proved to be overexpressed in aging and CRF kidney tissues,[27] making it particularly suitable as a trigger of prodrugs for CRF treatment. SA-β-gal is able to specifically hydrolyze the β-galactosidic bond of its substrates,[28] paving the way for researchers to design various chemical tools such as fluorescent probes and prodrugs to target SNCs. Up to now, dozens of β-galactosidase (β-gal) activable fluorescent probes have been constructed to identify SNCs.[29–37] The recent years have also witnessed a rapid development of β-gal activable prodrugs as senolytics for the treatment of age-related diseases.[38–42] However, to the best of our knowledge, theragnostic prodrugs capable of senolysis and identifying SNCs are rarely reported, and there is no research on the construction of SA-β-gal activable prodrugs as senolytics for the treatment of CRF.

To this end, we now report a new pharmacological strategy for senolysis towards CRF therapy. With an eye toward the ability of integrated fluorescence imaging and senolysis, a SA-β-gal activatable theragnostic prodrug **TSPD** was developed and used to treat CRF post-AKI for the first time. Three functional moieties were included in the design of **TSPD** (Scheme 1). First, the coumarin skeleton with good biocompatibility was adopted to serve as the fluorescence carrier. Second, into the skeleton, we installed a β-galactosidic bond, which can be selectively triggered by SA-β-gal, to achieve targeting and to quench fluorescence by blocking the intramolecular charge transfer (ICT) process occurring from the hydroxyl group. **TSPD** was finally obtained by introducing a prodrug structure with potential ability to release gemcitabine, a clinically used cytotoxic drug with potency toward SNCs.[41] **TSPD** can be selectively activated by SA-β-gal, resulting in the sequential release of both fluorophore for fluorescence imaging and free gemcitabine for chemotherapy. During this process, an active methylene benzopyrandione (MBP) intermediate was produced and was able to bioorthogonally form a covalent bond with the nucleophilic residue of surrounding proteins by an addition reaction. Such a design gives **TSPD** the ability to recognize SNCs at single-cell resolution and selectively eliminate β-gal-overexpressed cells whether transfected or senescent. Our *in vivo* studies confirm that **TSPD** can attenuate the degree of kidney injury and improve kidney function after AKI in mice through senolysis, supporting **TSPD** as a promising therapeutic drug for the management of CRF.

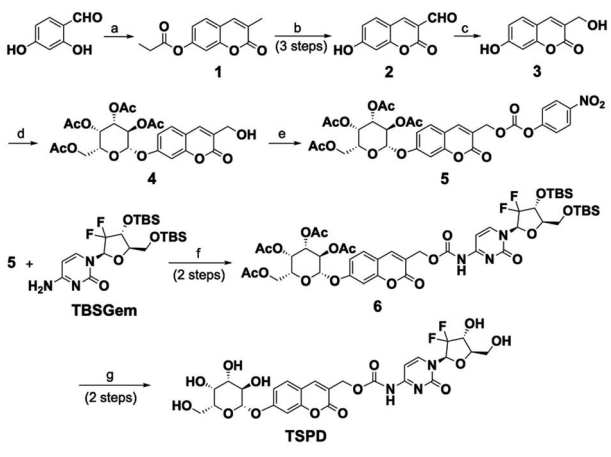

Scheme 1 Synthetic route for **TSPD**. Reagents and conditions: (a) $C_2H_5CO_2Na$, $(C_2H_5CO)_2O$, triethylamine, 170 °C, and 10 h. (b) (1) NBS, AIBN, CCl_4, 85 °C, and 12 h; (2) NaOAc, CH_3COOH, 120 °C, and 12 h; (3) HCl, r.t., and 12 h. (c) $NaBH_4$, MeOH, 0 °C, and 2 h. (d) 2,3,4,6-tetra-*O*-acetyl-α-D-galactopyranosyl bromide, Ag_2CO_3, HMTTA, dry CH_3CN, r.t., and 4 h. (e) 4-Nitrophenyl chloroformate, DIPEA, dry pyridine, THF, N_2, 0 °C, and 1 h. (f) (1) LiHMDS, N_2, dry THF, −78 °C, and 30 min; (2) dry THF, r.t., and 30 min. (g) (1) TBAF, dry THF, r.t., and 30 min; (2) CH_3ONa, dry CH_3OH, 0 °C, and 10 min.

Results and discussion

Synthesis and characterization of TSPD

The synthetic route for the theragnostic-senolytic-prodrug **TSPD** is depicted in Scheme 1. Compounds **1** and **2** were synthesized according to previously reported methods.[43,44] The fluorophore **3** was afforded by reducing compound **2** with $NaBH_4$ and was then reacted with commercially available 2,3,4,6-tetra-*O*-acetyl-α-D-galactopyranosyl bromide to give **4**. Compound **4** was then reacted with 4-nitrophenyl chloroformate and *N*,*N*-diisopropylethylamine (DIPEA) to give a reactive intermediate compound **5**, which was successively reacted with **TBSGem** to yield compound **6**. Finally, our desired prodrug **TSPD** was obtained as a light-yellow solid by removal of the *tert*-butyldimethylsilyl (TBS) and acetyl group of the compound **6**. The detailed synthetic procedures and original spectra are provided in the ESI.†

Spectroscopic response of TSPD toward β-gal

With the prodrug in hand, we first examined the spectral response of **TSPD** to *E. coli* β-gal, a bacterial enzyme widely used as an *in vitro* model of SA-β-gal. UV and fluorescence spectra were recorded under physiological conditions (37 °C, pH 7.4, 10 mmol L^{-1} phosphate buffer solution, PBS). As shown in Fig. 1A, the absorption bands of **TSPD** and compound **3** were centered at 294 nm and 324 nm, respectively. After incubation of **TSPD** with *E. coli* β-gal for 15 min, the absorption spectrum showed two new absorption peaks appearing at 272 nm and 324 nm. Upon the addition of *E. coli* β-gal, the fluorescence spectrum also changed, and about a 250-fold enhancement in emission intensity centered at 456 nm was observed, also the maximum emission wavelength of compound **3** occurred when excited at 360 nm (Fig. 1B). These results suggest that the coumarin fluorophore can be released after activation by β-gal. In addition, the time and concentration-dependent fluorescence enhancement of **TSPD** on the addition of *E. coli* β-gal were also investigated. As shown in Fig. 1C and D, the fluorescence intensity at 456 nm increased time-dependently and reached a plateau within 15 min. Upon stepwise addition of *E. coli* β-gal (0–5 U mL^{-1}), the fluorescence intensity at 456 nm increased concentration-dependently until reaching a saturation point at 5 U mL^{-1}. In addition, we performed the enzyme kinetics assay for the β-gal-catalyzed reaction (Fig. S1†). The catalytic efficiency

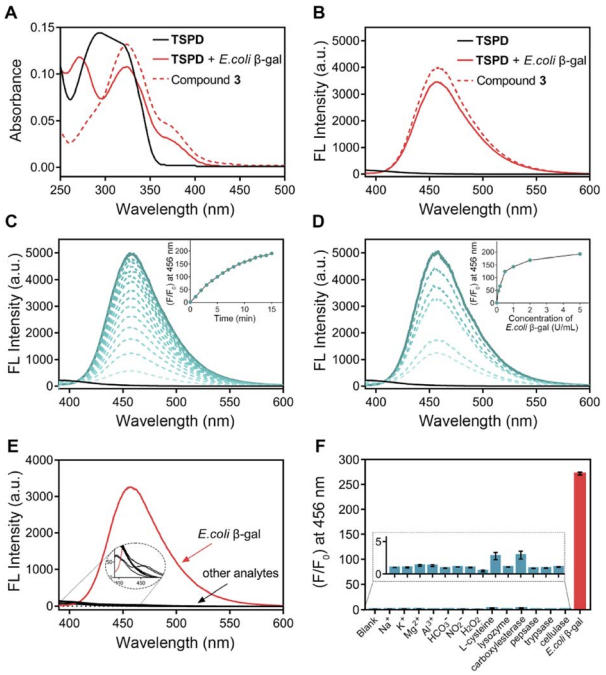

Fig. 1 (A) Absorption spectra of **TSPD** (10 μM), compound **3** (10 μM) and **TSPD** (10 μM) after incubation with *E. coli* β-gal (1 U mL^{-1}) at 37 °C for 15 min. (B) Fluorescence spectra of **TSPD** (10 μM), compound **3** (10 μM) and **TSPD** (10 μM) after incubation with *E. coli* β-gal (1 U mL^{-1}) at 37 °C for 15 min. (C) Time dependent fluorescence spectra of **TSPD** (10 μM) after incubation with *E. coli* β-gal (1 U mL^{-1}) at 37 °C. Inset: changes in fluorescence intensity at 456 nm as a function of time after *E. coli* β-gal (1 U mL^{-1}) treatment. (D) Fluorescence spectra of **TSPD** (10 μM) after incubation with *E. coli* β-gal (0–5 U mL^{-1}) at 37 °C for 15 min. Inset: changes in fluorescence intensity at 456 nm as a function of the *E. coli* β-gal concentration. (E) Fluorescence spectra and (F) fluorescence intensity at 456 nm of **TSPD** (10 μM) upon incubation with *E. coli* β-gal and other various biological analytes. (λ_{ex} = 360 nm, slit: 5 nm/5 nm, PMT: 500 V) (n = 3).

constant (k_{cat}/K_m) was calculated using the Michaelis–Menten equation and was found to be 0.98 μM^{-1} s^{-1} (k_{cat} = 23.95 s^{-1}, V_{max} = 0.103 μM s^{-1}). These results indicate that **TSPD** has rapid response ability and high sensitivity to β-gal.

Good anti-interference capability is very important for theragnostic prodrugs to target cellular enzymes in a complex environment. To assess whether other biologically relevant substances affect the fluorescence response of **TSPD** toward *E. coli* β-gal, we incubated **TSPD** with various possible cellular interferent analytes, including Na^+, K^+, Mg^{2+}, Al^{3+}, HCO_3^-, NO_2^-, H_2O_2, L-cysteine, lysozyme, carboxylesterase, pepsase, trypsase and cellulase. As depicted in Fig. 1E and F, for **TSPD**, significant fluorescence change at 456 nm can only be observed in the presence of *E. coli* β-gal, while there is no obvious enhancement for other potential interferents, confirming the high selectivity of **TSPD** toward β-gal.

Considering that SA-β-gal showed good enzyme activity at pH up to 6.0,[45] we subsequently evaluated the reaction of **TSPD** with *E. coli* β-gal in different pH values from 2.0 to 9.0. Fig. S2† shows the relationship between the fluorescence intensity at 456 nm and the environmental pH. The fluorescence intensity of **TSPD** was very weak and kept stable over the range of pH 2.0–9.0. After incubation of **TSPD** (10 μM) with *E. coli* β-gal (1 U mL^{-1}), the fluorescence intensity enhanced significantly over the pH range from 6.0 to 8.0, while at pH 9.0, this fluorescence intensity decreased sharply, which may be due to the decreased activity of *E. coli* β-gal in the unsuitable alkaline environment. Collectively, these results suggest that **TSPD** can detect *E. coli* β-gal at a pH ranging from 6.0 to 8.0, which is suitable for the detection of SA-β-gal activity in SNCs with lysosomal pH elevation.

Activation mechanism of the theragnostic prodrug

Based on the release mechanism of self-immolative linkers,[46] we propose that the β-D-galactosyl group of **TSPD** upon reaction with β-gal is cleaved to produce a phenolate, which then causes a self-immolation process to release the parent drug, gemcitabine, along with the active MBP capable to further react with surrounding nucleophiles to generate a fluorescence signal (Fig. 2A). To identify the response mechanism, high-performance liquid chromatography (HPLC) analysis was conducted. As shown in Fig. 2B, after incubation with *E. coli* β-gal, the HPLC peak for **TSPD** decreases, while the peaks corresponding to gemcitabine and compound **3** appear. The retention times of gemcitabine, compound **3** and **TSPD** in HPLC analysis are identified to be 7.12 min, 23.28 min and 26.55 min,

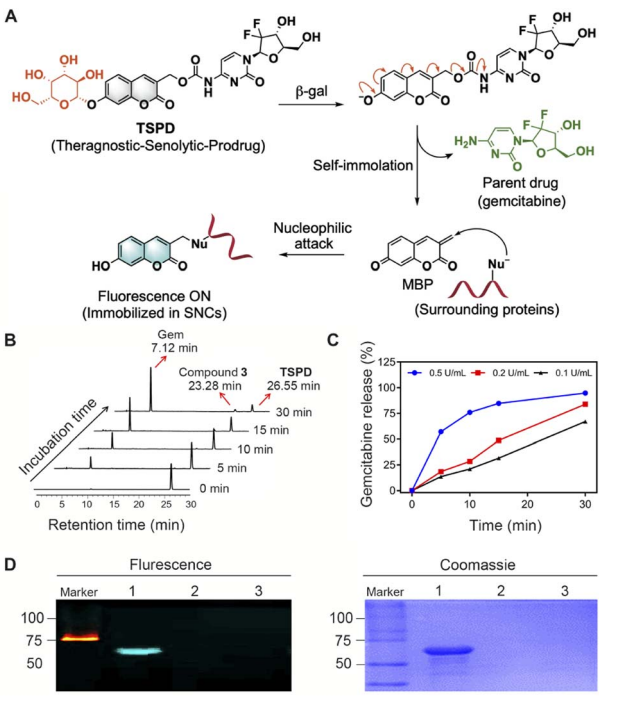

Fig. 2 (A) Proposed activation mechanism of **TSPD**. (B) HPLC analysis of **TSPD** (50 μM) in the presence of *E. coli* β-gal (0.1 U mL^{-1}) at 37 °C for 0–30 min (eluent A, MeOH; eluent B, water; 0–30 min, A/B = 10/90–80/20; flow rate = 1.0 mL min^{-1}). (C) Release of gemcitabine from **TSPD** in the presence of different concentrations of *E. coli* β-gal. (D) Fluorescence imaging (left) and Coomassie blue staining (right) of SDS-PAGE gel. **TSPD** (20 μM) was incubated with proteins at 37 °C for 0.5 h. 1, **TSPD** + *E. coli* β-gal (1 U mL^{-1}) + BSA (1 mg mL^{-1}); 2, **TSPD** + *E. coli* β-gal (1 U mL^{-1}); 3, **TSPD**; λ_{ex} = 365 nm.

respectively (Fig. S3A†). In this assay, gemcitabine was rapidly and completely released within a few minutes of incubation if the same proportion of **TSPD** to β-gal as that in fluorescence analysis assay was adopted (Fig. S4†). In order to obtain the drug release profiles *in vitro* with time, **TSPD** was then incubated with a lower concentration of *E. coli* β-gal, and the changes in the peaks of gemcitabine and compound **3** over time were monitored by HPLC. Of note, with the increase of incubation time, the peaks of gemcitabine and compound **3** as the reaction product of MBP with H_2O were subsequently heightened. The drug release profiles of **TSPD** (50 μM) after incubation with different concentrations of *E. coli* β-gal (0.1–0.5 U mL^{-1}) are displayed in Fig. 2C, S3B and S3C†. It can be seen that, with the increase of the concentration of *E. coli* β-gal, the released gemcitabine amount increases as well. These findings confirm the formation of gemcitabine and MBP during the reaction of **TSPD** with *E. coli* β-gal, which is also further supported by the high resolution mass spectrometry (HRMS) titration analysis (Fig. S5†).

Since the active MBP is able to react with surrounding nucleophiles including protein nucleophilic residues, we next investigated the protein fluorescent labeling ability of **TSPD** by gel imaging. Bovine serum albumin (BSA) was chosen as the model because the protein contains a strongly nucleophilic free sulfhydryl group. Incubation of BSA (1 mg mL^{-1}) with **TSPD** (20 μM) in the presence of *E. coli* β-gal (1 U mL^{-1}) elicited a clear fluorescent band (Fig. 2D), while no fluorescent signal is generated in the absence of BSA. These results indicate that **TSPD** possesses the ability to fluorescently label proteins and the potential of single-cell resolution imaging.

Fluorescence imaging and selective death in β-gal-overexpressed cells

Since **TSPD** showed the excellent fluorescence response to β-gal and the effective drug release behavior in the above *in vitro* assays, we next assessed its capability to visualize endogenous β-gal activity both in *LacZ*-transfected cells and in drug-induced SNCs. First, we constructed A549 cells with high expression of *E. coli* β-gal through the transfection of the *LacZ* gene. The overexpression of *E. coli* β-gal was verified by using a western blot assay (Fig. S6E and S6F†). The normal A549 cells (control group) were set as the *LacZ*-(−) group. The *LacZ*-(−) and *LacZ*-(+) A549 cells were respectively incubated with **TSPD** (20 μM) at 37 °C for 4 h and then imaged with a Nikon TS2R microscope. As shown in Fig. S6A†, the fluorescence within the *LacZ*-(−) A549 cells was barely observed, while the *LacZ*-(+) A549 cells showed an obvious fluorescence signal in the cyan channel. Next, we treated *LacZ*-(−) and *LacZ*-(+) A549 cells with various concentrations of **TSPD** to test whether **TSPD** could selectively induce the death in β-gal-overexpressed cells. As expected, the results confirm that **TSPD** has higher cytotoxicity to *LacZ*-(+) A549 cells than *LacZ*-(−) A549 cells (Fig. S7A†). However, the parent drug gemcitabine was highly toxic to both *LacZ*-(−) and *LacZ*-(+) A549 cells (Fig. S7C†). To further understand the application of **TSPD** in the detection of cellular SA-β-gal activity, we conducted other imaging experiments on Mitomycin C (MitoC) induced SNCs. MitoC is a well-known DNA damage agent able to induce senescence in A549 cells.[47] The cytotoxicity experiments of MitoC to cells were first performed to select a safe dose to induce senescence (Fig. S8†). After being treated with MitoC (0.5 μM) for 48 h and further cultivated in fresh Ham's F12K medium for another 48 h, A549 cells became senescent and expressed enhanced levels of SA-β-gal, which was verified using X-gal staining (Fig. S6C and S6D†). The overexpression of p53 and p21, other two key cellular senescence biomarkers, in MitoC-induced senescent A549 cells was also verified by a western blot assay (Fig. S6E, S6G and S6H†) to guarantee the reliability of this technique for inducing cell senescence. The senescent A549 cells and the uninduced A549 cells as controls were separately incubated with **TSPD** (20 μM) for 4 h and then imaged. As shown in Fig. S6B†, the control group exhibited a negligible fluorescence response, while the fluorescence intensity in SNCs increased significantly and was proportional to the **TSPD** concentration (Fig. S9†). Furthermore, the

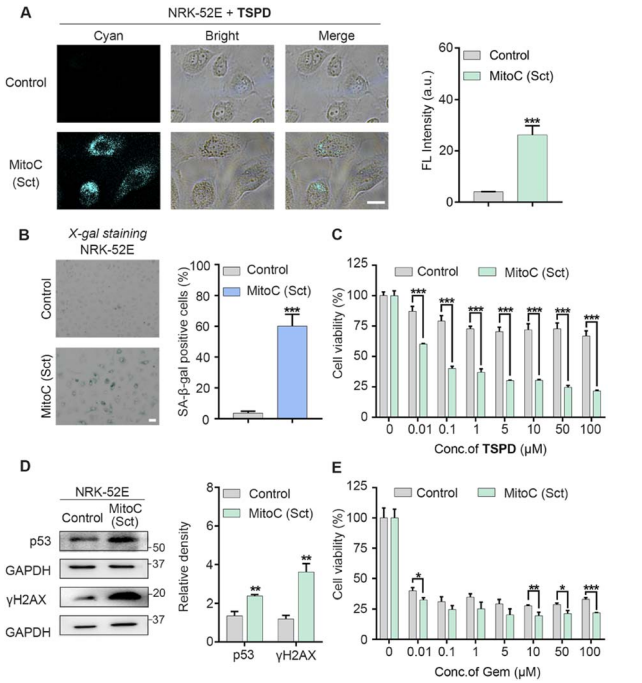

Fig. 3 (A) Fluorescence images of uninduced NRK-52E cells (control) and MitoC-induced senescent (sct) NRK-52E cells after incubation with TSPD (20 μM) for 4 h. Quantification of relative fluorescence intensity of (A) is on the right ($n = 3$). Scale bar = 20 μm. (B) X-gal staining images of uninduced NRK-52E cells and MitoC-induced senescent NRK-52E cells. The average percentage of SA-β-gal positive cells of (B) is on the right ($n = 3$). Scale bar = 20 μm. (C) Quantification of cell viability of uninduced NRK-52E cells and MitoC-induced senescent NRK-52E cells incubated with increasing concentrations of TSPD for 2 days ($n = 3$). (D) Western blotting analysis of p53 and γH2AX in uninduced NRK-52E cells and MitoC-induced senescent NRK-52E cells. GAPDH was chosen as an internal reference ($n = 2$). (E) Quantification of cell viability of uninduced NRK-52E cells and MitoC-induced senescent NRK-52E cells incubated with increasing concentrations of gemcitabine for 2 days ($n = 3$). Significant differences (*$P < 0.05$, **$P < 0.01$, and ***$P < 0.001$) are analyzed with the *t*-test.

quantitative results of the fluorescence (Fig. S6B†) strongly corresponded to the percentage of SA-β-gal positive cells (Fig. S6D†). Such results indicate that **TSPD** was able to accurately differentiate SNCs from non-senescent cells. Next, the ability of **TSPD** in lysosomal localization was evaluated by co-staining with LysoTracker Green and MitoTracker Green, respectively, in MitoC-induced senescent A549 cells. As shown in Fig. S10†, **TSPD** shows nice correspondence with LysoTracker with a Pearson's correlation coefficient (PCC) value as high as 0.98, while with MitoTracker with a low PCC value of 0.67, supporting that our fluorophore predominantly accumulated in the lysosomes of SNCs enriched with lysosomal SA-β-gal. Next, the CCK-8 assay was conducted to evaluate the efficacy of **TSPD** in selective elimination of SNCs. As can be seen in Fig. S7B†, **TSPD** exhibited potent cytotoxicity toward MitoC-induced SNCs. When the concentration of **TSPD** was at 5 μM, the viability of SNCs was below 25%, while only marginal cytotoxicity can be observed in control cells. Unlike **TSPD**, the same dose of the parent drug gemcitabine killed both uninduced cells and MitoC-induced SNCs without selectivity (Fig. S7D†). These results, together with the aforementioned data, suggest that **TSPD** could be selectively activated to release the fluorophore and gemcitabine in SNCs and might have the potential to serve as an effective senolytic drug for the treatment of age-related diseases.

We then set our sights on the treatment of CRF, which is a disease closely related to senescence, as explained above. NRK-52E cells, a kind of rat renal tubular epithelial cell, were employed to verify our theragnostic prodrug strategy. The senescent NRK-52E cells were obtained by the same method as the senescent A549 cells and verified by the overexpression of senescence-associated protein markers in X-gal staining and western blot assays (Fig. 3B and D). After incubation with **TSPD**, no significant fluorescence signal in uninduced NRK-52E cells was observed, while the fluorescence in senescent NRK-52E cells enhanced significantly (Fig. 3A), confirming the targeting of **TSPD** to senescent kidney cells. Furthermore, the cell viability test of **TSPD** was performed by CCK-8 assay. As shown in Fig. 3C, **TSPD** could selectively remove the senescent NRK-52E cells even at a low concentration of 0.01 μM, showing an excellent senolytic ability. As expected, the parent drug gemcitabine without this ability showed high cytotoxicity to both uninduced cells and MitoC-induced SNCs (Fig. 3E). All the above findings in kidney cells support the therapeutic potential of our theragnostic prodrug strategy for CRF.

Senolysis-based CRF therapy *in vivo*

We next examined the therapeutic effect of **TSPD** on CRF *in vivo* by employing a renal unilateral ischemia reperfusion injury (UIRI) murine model (Fig. 4A). UIRI is a severe clinical AKI with a high risk of progression to CRF and associated with high mortality.[48] To evaluate the safety of **TSPD** *in vivo*, we carried out a subacute toxicity test in mice (Fig. S11 and S12†). The treatment of **TSPD** displayed no obvious toxicity even at a high dose of 25 mg kg^{-1} for two weeks from the results of body weight, serum biochemical test and HE staining assay of vital organs. We treated the kidney-injured mice with the vehicle, gemcitabine or **TSPD** *via* intraperitoneal injection (twice a week for three weeks). After 21 days, the kidneys of these treated mice were harvested for analysis. Meanwhile, the levels of blood urea nitrogen (BUN) and serum creatinine (SCr) were measured to assess renal function of mice in each group. To our delight, the results indicate that both the BUN and SCr levels upregulated in UIRI mice were reduced to the normal range after treatment with **TSPD** (Fig. 4D and E), suggesting that the declined renal function caused by UIRI had been restored. Then, we observed the color and size of the kidneys. As illustrated in Fig. 4C and S13,† the kidneys in the vehicle group (UIRI) were significantly smaller and lighter than those in the UIRI group using **TSPD** (5 mg kg^{-1}), indicating that a significant improvement was observed after treatment, while treatment with **TSPD** at a low concentration (1 mg kg^{-1}) or gemcitabine (1 mg kg^{-1} or 5 mg kg^{-1}) failed to improve the morphology of kidney. Then we tested whether **TSPD** could reduce renal senescence post-UIRI by staining renal sections with anti-lamin B1 antibody and X-gal, respectively. A reduction in the abundance of lamin B1 protein in the nuclear envelope has been considered as a characteristic of senescence.[25,49] As seen in Fig. 4B, treatment with **TSPD** (5 mg kg^{-1}) remarkably increased the nuclear lamin B1 content, while the gemcitabine-treated mice group showed scant improvement compared with the vehicle group. In addition, treatment with **TSPD** decreased the percentage of SA-β-gal-positive cells in kidney by 1.56-fold compared to that without **TSPD** incubation, and by 1.23-fold compared to that with gemcitabine treatment (Fig. 4F). Taken together, our findings indicate that **TSPD** has the potential to eliminate SA-β-gal-positive cells and increase another type of senescence-negatively-associated marker lamin B1 in damaged kidneys. Importantly, although gemcitabine had some effect on senolysis due to its broad spectrum of cytotoxicity, its effect was far lower than that of **TSPD**. This should be attributed to our prodrug design strategy that endows **TSPD** with the ability to be selectively activated and accumulated in SNCs.

As renal tubulointerstitial fibrosis is a prominent pathological characteristic of CRF,[20,50] we next investigated whether **TSPD** can alleviate post-UIRI renal fibrosis. As shown in Fig. 4G, the degree of renal fibrosis in the vehicle-treated kidneys, as measured by picrosirius red (PSR) staining, was higher than that in the sham group and could be significantly reduced by administration of **TSPD** (5 mg kg^{-1}), while there was a negligible difference in the degree of fibrosis between gemcitabine-treated and vehicle-treated groups. Since the expression of cellular Ki67, a cell proliferation marker, can be increased after injury,[21,51–53] we then used this marker for the evaluation of our molecule. As shown in Fig. 4H, the proliferative cells, represented by Ki67 staining, increased significantly in the UIRI group, and the number of these Ki67-positive cells was markedly reduced after treatment with only **TSPD**, rather than gemcitabine. These data suggest that the **TSPD**-treated tubular cells have a response to injury and can enter the proliferative cycle again from the quiescent state. Kidney injury molecule 1 (KIM-1) participates in differentiation, proliferation and migration of renal tubule epithelial cells and can be used as an early

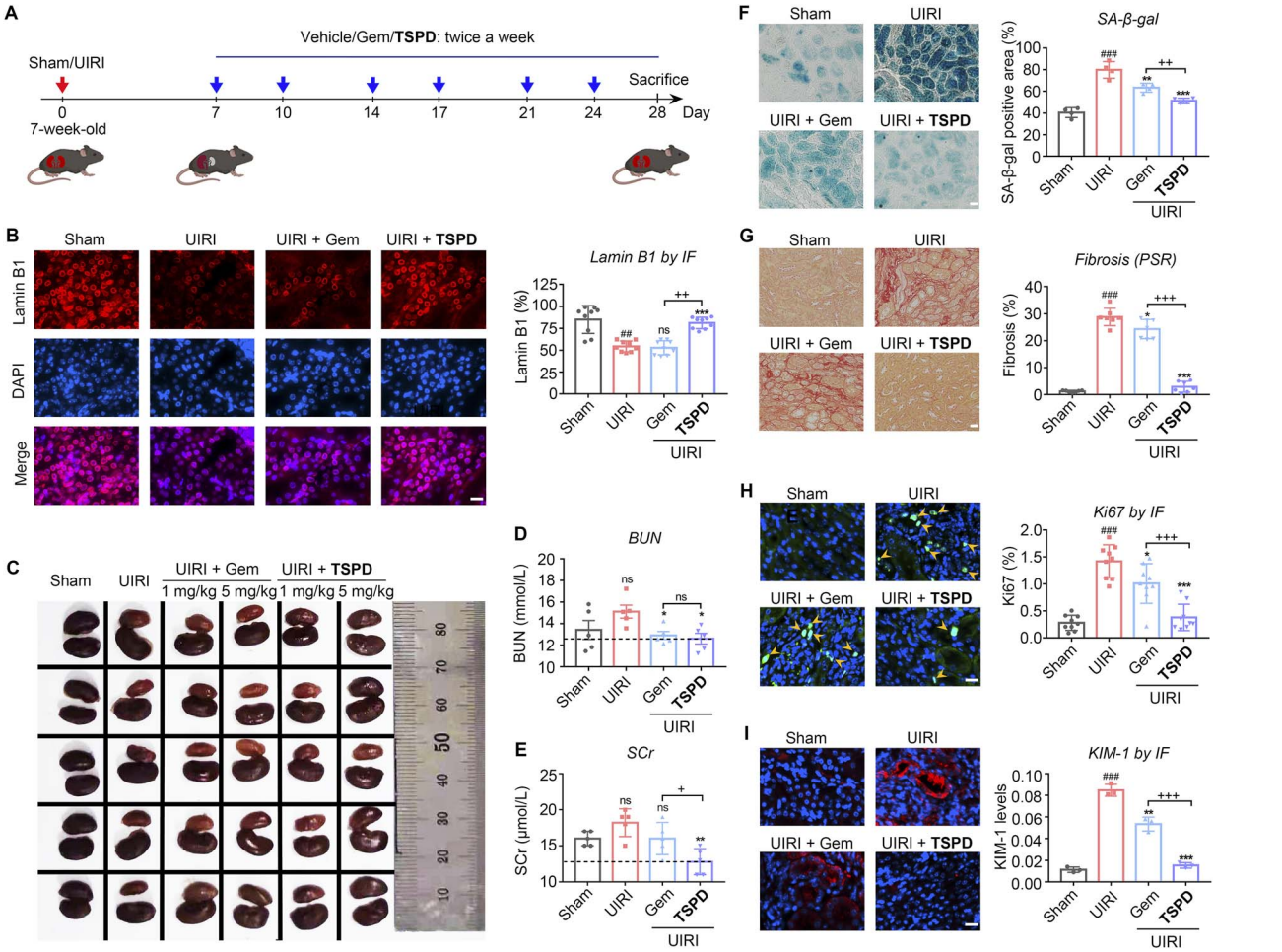

Fig. 4 (A) Experimental design for renal unilateral ischemia reperfusion injury (UIRI). Mice (7 weeks-old) were subjected to renal unilateral ischemia reperfusion injury surgery or sham surgery 7 days before drug treatment. UIRI mice were intraperitoneally injected with gemcitabine (1 mg kg^{-1} and 5 mg kg^{-1}), **TSPD** (1 mg kg^{-1} and 5 mg kg^{-1}) or vehicle (2% DMSO, 90% PBS, 4% Tween-80, and 4% polyethylene glycol) twice a week for three weeks; sham surgery mice were treated with vehicle in the same way. (B) Representative images (left) and quantification (right) of lamin B1 staining of kidneys from sham or UIRI mice after vehicle, gemcitabine or **TSPD** treatment ($n = 9$ for each group). (C) Representative images of kidneys from sham or UIRI mice after vehicle, gemcitabine or **TSPD** treatment ($n = 5$ for each group). (D and E) Serum biochemical test. The levels of blood urea nitrogen (BUN) and serum creatinine (SCr) in sham or UIRI mice after vehicle, gemcitabine or **TSPD** treatment as shown ($n = 5$ for each group). (F) Representative images (left) and quantification (right) of SA-β-gal staining of kidneys from sham or UIRI mice after vehicle, gemcitabine or **TSPD** treatment ($n = 4$ for each group). (G) PSR ($n = 7$ for each group). (H) Ki67 ($n = 9$ for each group). (I) KIM-1 ($n = 3$ for each group). Scale bar = 20 μm. Significant differences ($^{\#\#}P < 0.01$ and $^{\#\#\#}P < 0.001$, compared with the Sham group, $^{*}P < 0.05$ and $^{***}P < 0.001$, compared with the UIRI group, and $^{+}P < 0.05$, $^{++}P < 0.01$, and $^{+++}P < 0.001$, compared with the UIRI + Gem group) are analyzed with the *t*-test.

detection indicator of kidney disease because of its acute up-regulation in damaged proximal tubules.[9,54–56] We then quantified the level of KIM-1 protein after UIRI in diseased kidneys. As shown in Fig. 4I, the KIM-1 level was significantly reduced in **TSPD**-treated UIRI *versus* vehicle-treated UIRI kidneys. This indicates that it is reliable to consume KIM-1, the marker of progressive tubular injury, through **TSPD**-mediated senolysis *in vivo*, and the senolytic therapy with **TSPD** is expected to prevent the CRF progression by improving injury. Instead, positive signals of KIM-1 were observed in the same figure (Fig. 4I) with high intensity in the gemcitabine-treated group, showing poor therapeutic efficacy of gemcitabine instead of **TSPD**. From the above results, **TSPD**, as a senolytic drug, has played a good role in alleviating CRF post-AKI and improving renal function, which confirms the advancement of our prodrug design strategy for the treatment of renal failure.

Conclusions

Using a senolysis-based molecular design strategy, we have successfully designed and synthesized a pioneering theragnostic prodrug **TSPD** towards CRF. The present prodrug reasonably integrates the parent drug gemcitabine structure and a potential fluorophore skeleton with the enzyme substrate of β-gal to achieve the precise theragnosis for CRF. With this creative design, **TSPD** has shown its superior ability not only to track SNCs at single-cell resolution by SA-β-gal-triggered fluorescent labelling of proteins, but also to be selectively activated

by SA-β-gal to release the cytotoxic parent drug, gemcitabine, into the CRF kidney where renal failure causes premature senescence and SNC accumulation. This capability of **TSPD** has been demonstrated by selective imaging of SA-β-gal in SNCs and excellent senolysis-based therapeutic activity specific to mice with CRF. As such, our theragnostic prodrug **TSPD** has proved to be unprecedentedly effective in the specific treatment of CRF in mice, providing a promising molecular approach and the conclusive evidence for treating renal failure by senolysis.

Data availability

The data supporting this article have been uploaded as part of the ESI.†

Author contributions

Y. S. and X. L. carried out the synthetic work. Y. S. and D. S. carried out the spectroscopic measurements and cell imaging experiments. W. L. and X. L. (Xiaokang Li) carried out the cytotoxicity test. T. S., S. Q., and X. C. carried out the animal experiments. Y. G., J. L., Y. S., X. L. and D. S. wrote and revised the manuscript. Y. G. and J. L. supervised the research. Y. G. and J. L. conceived and designed the project.

Conflicts of interest

The authors declare that they have no competing financial interests.

Acknowledgements

The authors are thankful for the financial support from the Natural Science Foundation of China (22037002, 22007032 and 21977082), the Natural Science Basic Research Program of Shaanxi (2020JC-38), the Innovation Program of Shanghai Municipal Education Commission (2021-01-07-00-02-E00104), the Shanghai Frontier Science Research Base of Optogenetic Techniques for Cell Metabolism (2021 Sci & Tech 03-28), the Innovative Research Team of High-level Local Universities in Shanghai (SHSMU-ZDCX20212702), the Chinese Special Fund for State Key Laboratory of Bioreactor Engineering (2060204), the Chinese Postdoctoral Science Foundation, China (No. 2019M660083), the Postdoctoral Innovation Talent Support Program, China (No. BX20200131), and the Shanghai Sailing Program, China (No. 20YF1411200). Male and female ICR mice (8 weeks, weighing 20–24 g) were purchased from Zhejiang Vital River Laboratory Animal Technology Co., Ltd. and male C57BL/6 mice (7 weeks, weighing 20–22 g) were purchased from Shanghai Jiesijie Laboratory Animal Co., Ltd. All mice were maintained under controlled temperature (22–23 °C) and light (12:12 hours of light–dark cycles) conditions at the animal center, approved by the Institutional Animal Care and Use Committees of Tongji University in compliance with Chinese law for experimental animals with an approval number of SYXK (Shanghai) 2020–0002.

References

1 I. N. Price and A. F. Wood, *Br. J. Nurs.*, 2022, **31**, 124–134.
2 K. Kalantar-Zadeh, T. H. Jafar, D. Nitsch, B. L. Neuen and V. Perkovic, *Lancet*, 2021, **398**, 786–802.
3 T. K. Chen, D. H. Knicely and M. E. Grams, *Jama*, 2019, **322**, 1294–1304.
4 V. Jha, G. Garcia-Garcia, K. Iseki, Z. Li, S. Naicker, B. Plattner, R. Saran, A. Y.-M. Wang and C.-W. Yang, *Lancet*, 2013, **382**, 260–272.
5 Y. Xie, B. Bowe, A. H. Mokdad, H. Xian, Y. Yan, T. Li, G. Maddukuri, C. Y. Tsai, T. Floyd and Z. Al-Aly, *Kidney Int.*, 2018, **94**, 567–581.
6 J. A. Kellum, P. Romagnani, G. Ashuntantang, C. Ronco, A. Zarbock and H.-J. Anders, *Nat. Rev. Dis. Prim.*, 2021, **7**, 52.
7 J. A. Neyra and L. S. Chawla, *Crit. Care Clin.*, 2021, **37**, 453–474.
8 L. S. Chawla, P. W. Eggers, R. A. Star and P. L. Kimmel, *N. Engl. J. Med.*, 2014, **371**, 58–66.
9 D. A. Ferenbach and J. V. Bonventre, *Nat. Rev. Nephrol.*, 2015, **11**, 264–276.
10 P. Buendia, J. Carracedo, S. Soriano, J. A. Madueno, A. Ortiz, A. Martin-Malo, P. Aljama and R. Ramirez, *J. Gerontol. Biol. Med. Sci.*, 2015, **70**, 1198–1209.
11 S. Yamada, N. Tatsumoto, M. Tokumoto, H. Noguchi, H. Ooboshi, T. Kitazono and K. Tsuruya, *Calcif. Tissue Int.*, 2015, **96**, 347–358.
12 B. M. Klinkhammer, R. Kramann, M. Mallau, A. Makowska, C. R. van Roeyen, S. Rong, E. B. Buecher, P. Boor, K. Kovacova, S. Zok, B. Denecke, E. Stuettgen, S. Otten, J. Floege and U. Kunter, *PLoS One*, 2014, **9**, e92115.
13 B. G. Childs, M. Gluscevic, D. J. Baker, R. M. Laberge, D. Marquess, J. Dananberg and J. M. van Deursen, *Nat. Rev. Drug Discovery*, 2017, **16**, 718–735.
14 A. Calcinotto, J. Kohli, E. Zagato, L. Pellegrini, M. Demaria and A. Alimonti, *Physiol. Rev.*, 2019, **99**, 1047–1078.
15 I. Sturmlechner, M. Durik, C. J. Sieben, D. J. Baker and J. M. van Deursen, *Nat. Rev. Nephrol.*, 2017, **13**, 77–89.
16 M. H. Docherty, E. D. O'Sullivan, J. V. Bonventre and D. A. Ferenbach, *J. Am. Soc. Nephrol.*, 2019, **30**, 726–736.
17 M. Matjusaitis, G. Chin, E. A. Sarnoski and A. Stolzing, *Ageing Res. Rev.*, 2016, **29**, 1–12.
18 B. Lozano-Torres, A. Estepa-Fernández, M. Rovira, M. Orzáez, M. Serrano, R. Martínez-Máñez and F. Sancenón, *Nat. Rev. Chem.*, 2019, **3**, 426–441.
19 T. Y. Yoshikazu Johmura, S. Omori, T.-W. Wang, Y. Sugiura, M. Matsumoto, N. Suzuki, S. Kumamoto, K. Yamaguchi, S. Hatakeyama, T. Takami, R. Yamaguchi, E. Shimizu, K. Ikeda, N. Okahashi, R. Mikawa, M. Suematsu, M. Arita, M. Sugimoto, K. I. Nakayama, Y. Furukawa, S. Imoto and M. Nakanishi, *Science*, 2021, **371**, 265–270.
20 C. Li, Y. Shen, L. Huang, C. Liu and J. Wang, *FASEB J.*, 2021, **35**, e21229.
21 K. J. Mylonas, E. D. O'Sullivan, D. Humphries, D. P. Baird, M. H. Docherty, S. A. Neely, P. J. Krimpenfort, A. Melk, R. Schmitt, S. Ferreira-Gonzalez, S. J. Forbes, J. Hughes and D. A. Ferenbach, *Sci. Transl. Med.*, 2021, **13**, eabb0203.

22 E. González-Gualda, A. G. Baker, L. Fruk and D. Muñoz-Espín, *FEBS J.*, 2021, **288**, 56–80.
23 D. J. Baker, T. Wijshake, T. Tchkonia, N. K. LeBrasseur, B. G. Childs, B. van de Sluis, J. L. Kirkland and J. M. van Deursen, *Nature*, 2011, **479**, 232–236.
24 G. P. Dimri, X. Lee, G. Basile, M. Acosta, G. Scott, C. Roskelley, E. E. Medrano, M. Linskens, I. Rubelj, O. Pereira-Smith, *et al.*, *Proc. Natl. Acad. Sci. U. S. A.*, 1995, **92**, 9363–9367.
25 A. Freund, R.-M. Laberge, M. Demaria and J. Campisi, *Mol. Biol. Cell*, 2012, **23**, 2066–2075.
26 J. A. de Mera-Rodriguez, G. Alvarez-Hernan, Y. Ganan, G. Martin-Partido, J. Rodriguez-Leon and J. Francisco-Morcillo, *Front. Cell Dev. Biol.*, 2021, **9**, 623175.
27 F. A. Valentijn, L. L. Falke, T. Q. Nguyen and R. Goldschmeding, *J. Cell Commun. Signaling*, 2018, **12**, 69–82.
28 L. Lu, L. Guo, K. Wang, Y. Liu and M. Xiao, *Biotechnol. Adv.*, 2020, **39**, 107465.
29 W. Qiu, X. Li, D. Shi, X. Li, Y. Gao, J. Li, F. Mao, Y. Guo and J. Li, *Dyes Pigm.*, 2020, **182**, 108657.
30 Y. Gao, Y. Hu, Q. Liu, X. Li, X. Li, C. Y. Kim, T. D. James, J. Li, X. Chen and Y. Guo, *Angew. Chem., Int. Ed.*, 2021, **60**, 10756–10765.
31 Z. Li, J. Cheng, L. Huang, W. Li, Y. Zhao and W. Lin, *Anal. Chem.*, 2021, **93**, 13800–13806.
32 B. Lozano-Torres, J. F. Blandez, I. Galiana, J. A. Lopez-Dominguez, M. Rovira, M. Paez-Ribes, E. González-Gualda, D. Muñoz-Espín, M. Serrano, F. Sancenón and R. Martínez-Máñez, *Anal. Chem.*, 2021, **93**, 3052–3060.
33 B. Lozano-Torres, I. Galiana, M. Rovira, E. Garrido, S. Chaib, A. Bernardos, D. Muñoz-Espín, M. Serrano, R. Martínez-Máñez and F. Sancenón, *J. Am. Chem. Soc.*, 2017, **139**, 8808–8811.
34 D. Shi, W. Liu, G. Wang, Y. Guo and J. Li, *Acta Materia Medica*, 2022, **1**, 4–23.
35 X. Li, W. Qiu, J. Li, X. Chen, Y. Hu, Y. Gao, D. Shi, X. Li, H. Lin, Z. Hu, G. Dong, C. Sheng, B. Jiang, C. Xia, C. Y. Kim, Y. Guo and J. Li, *Chem. Sci.*, 2020, **11**, 7292–7301.
36 H. W. Lee, V. Juvekar, D. J. Lee, S. M. Kim and H. M. Kim, *Anal. Chem.*, 2021, **93**, 14778–14783.
37 H. W. Lee, C. H. Heo, D. Sen, H. O. Byun, I. H. Kwak, G. Yoon and H. M. Kim, *Anal. Chem.*, 2014, **86**, 10001–10005.
38 A. Guerrero, R. Guiho, N. Herranz, A. Uren, D. J. Withers, J. P. Martínez-Barbera, L. F. Tietze and J. Gil, *Aging Cell*, 2020, **19**, e13133.
39 E. González-Gualda, M. Pàez-Ribes, B. Lozano-Torres, D. Macias, J. R. Wilson 3rd, C. González-López, H. L. Ou, S. Mirón-Barroso, Z. Zhang, A. Lérida-Viso, J. F. Blandez, A. Bernardos, F. Sancenón, M. Rovira, L. Fruk, C. P. Martins, M. Serrano, G. J. Doherty, R. Martínez-Máñez and D. Muñoz-Espín, *Aging Cell*, 2020, **19**, e13142.
40 Y. Xia, J. Li, L. Wang, X. Luo, Y. Xie and Y. Liu, *Angew. Chem., Int. Ed.*, 2022, **61**, e202115764.
41 Y. Cai, H. Zhou, Y. Zhu, Q. Sun, Y. Ji, A. Xue, Y. Wang, W. Chen, X. Yu, L. Wang, H. Chen, C. Li, T. Luo and H. Deng, *Cell Res.*, 2020, **30**, 574–589.
42 L. Yang, G. Liu, Q. Chen, Y. Wan, Z. Liu, J. Zhang, C. Huang, Z. Xu, S. Li, C.-S. Lee, L. Zhang and H. Sun, *Anal. Chem.*, 2022, **94**, 5425–5431.
43 C. Zhang, K. Yang, S. Yu, J. Su, S. Yuan, J. Han, Y. Chen, J. Gu, T. Zhou, R. Bai and Y. Xie, *Eur. J. Med. Chem.*, 2019, **180**, 367–382.
44 H.-Y. Tang, Y. Gao, B. Li, C.-W. Li and Y. Guo, *Sens. Actuators, B*, 2018, **270**, 562–569.
45 B. Y. Lee, J. A. Han, J. S. Im, A. Morrone, K. Johung, E. C. Goodwin, W. J. Kleijer, D. DiMaio and E. S. Hwang, *Aging Cell*, 2006, **5**, 187–195.
46 J. Yan, S. Lee, A. Zhang and J. Yoon, *Chem. Soc. Rev.*, 2018, **47**, 6900–6916.
47 E. McKenna, F. Traganos, H. Zhao and Z. Darzynkiewicz, *Cell Cycle*, 2012, **11**, 3132–3140.
48 J. V. Bonventre and L. Yang, *J. Clin. Invest.*, 2011, **121**, 4210–4221.
49 T. Shimi, V. Butin-Israeli, S. A. Adam, R. B. Hamanaka, A. E. Goldman, C. A. Lucas, D. K. Shumaker, S. T. Kosak, N. S. Chandel and R. D. Goldman, *Genes Dev.*, 2011, **25**, 2579–2593.
50 B. J. Ballermann and M. Obeidat, *Kidney Int. Suppl.*, 2014, **4**, 45–52.
51 T. Koyano, M. Namba, T. Kobayashi, K. Nakakuni, D. Nakano, M. Fukushima, A. Nishiyama and M. Matsuyama, *Sci. Rep.*, 2019, **9**, 12059.
52 N. Alessio, D. Aprile, S. Cappabianca, G. Peluso, G. Di Bernardo and U. Galderisi, *Int. J. Mol. Sci.*, 2021, **22**, 3102.
53 T. Kusaba, M. Lalli, R. Kramann, A. Kobayashi and B. D. Humphreys, *Proc. Natl. Acad. Sci. U. S. A.*, 2014, **111**, 1527–1532.
54 L. Yang, C. R. Brooks, S. Xiao, V. Sabbisetti, M. Y. Yeung, L. L. Hsiao, T. Ichimura, V. Kuchroo and J. V. Bonventre, *J. Clin. Invest.*, 2015, **125**, 1620–1636.
55 V. S. Sabbisetti, S. S. Waikar, D. J. Antoine, A. Smiles, C. Wang, A. Ravisankar, K. Ito, S. Sharma, S. Ramadesikan, M. Lee, R. Briskin, P. L. De Jager, T. T. Ngo, M. Radlinski, J. W. Dear, K. B. Park, R. Betensky, A. S. Krolewski and J. V. Bonventre, *J. Am. Soc. Nephrol.*, 2014, **25**, 2177–2186.
56 J. V. Bonventre, *Nephrol., Dial., Transplant.*, 2009, **24**, 3265–3268.